THE JOURNAL OF BIOLOGICAL CHEMISTRY VOL. 287, NO. 9, pp. 6851–6859, February 24, 2012

Quaternary Structure Controls Ligand Dynamics in Soluble Guanylate Cyclase*[S]

Received for publication, August 30, 2011, and in revised form, January 3, 2012 Published, JBC Papers in Press, January 4, 2012, DOI 10.1074/jbc.M111.299297

Byung-Kuk Yoo, Isabelle Lamarre, Jean-Louis Martin, and Michel Negrerie[1]

From the Laboratoire d'Optique et Biosciences, INSERM U696, CNRS UMR 7645 Ecole Polytechnique, 91128 Palaiseau, France

Background: NO and CO dynamics are compared in soluble guanylate cyclase and isolated heme domain.
Results: CO geminately rebinds to the isolated heme domain β_1(190), contrary to entire sGC. Photo-oxidation of β_1(190) heme may occur.
Conclusion: The isolated heme domain β_1(190) has a different reactivity than full-length sGC.
Significance: The structural strains between domains in the full-length protein are crucial for its functioning.

Soluble guanylate cyclase (sGC) is the mammalian endogenous nitric oxide (NO) receptor. The mechanisms of activation and deactivation of this heterodimeric enzyme are unknown. For deciphering them, functional domains can be overexpressed. We have probed the dynamics of the diatomic ligands NO and CO within the isolated heme domain β_1(190) of human sGC by piconanosecond absorption spectroscopy. After photoexcitation of nitrosylated sGC, only NO geminate rebinding occurs in 7.5 ps. In β_1(190), both photo-dissociation of 5c-NO and photo-oxidation occur, contrary to sGC, followed by NO rebinding (7 ps) and back-reduction (230 ps and 2 ns). In full-length sGC, CO geminate rebinding to the heme does not occur. In contrast, CO geminately rebinds to β_1(190) with fast multiphasic process (35, 171, and 18 ns). We measured the bimolecular association rates $k_{on} = 0.075 \pm 0.01 \times 10^6\ \mathrm{M}^{-1}\cdot\mathrm{s}^{-1}$ for sGC and $0.83 \pm 0.1 \times 10^6\ \mathrm{M}^{-1}\cdot\mathrm{s}^{-1}$ for β_1(190). These different dynamics reflect conformational changes and less proximal constraints in the isolated heme domain with respect to the dimeric native sGC. We concluded that the α-subunit and the β_1(191–619) domain exert structural strains on the heme domain. These strains are likely involved in the transmission of the energy and relaxation toward the activated state after Fe^{2+}-His bond breaking. This also reveals the heme domain plasticity modulated by the associated domains and subunit.

Soluble guanylate cyclase (sGC),[2] expressed in different cell types, is the mammalian receptor of the endogenous messenger nitric oxide (NO) and catalyzes the formation of the second messenger cGMP from GTP after activation by NO binding (1–3). It plays a critical role in regulation of vascular blood pressure (4), lung airway relaxation (5), and immune response (6). In heterodimeric sGC, the GTP catalytic site is located presumably at the interface between both subunits, whereas the sensing domain in β-subunit contains the heme group necessary for NO binding. The first internal molecular event correlated with sGC activation is the cleavage of the heme-proximal His covalent bond induced by trans effect after NO binding (7). Because the sensing heme domain and the GTP-binding catalytic site are located remotely, we must assume a "cross-talk" between both subunits for this allosteric regulation, which results in an increase of catalytic activity. Thus, the Fe^{2+}-His bond cleavage necessarily triggers structural changes within the dimeric protein, mediated by interactions between subunits. In the absence of three-dimensional crystal structure of heterodimeric sGC, the heme domain of the β-subunit was modeled from the structure of homologous bacterial NO sensors (8–10), and several studies used these sensors as structural models for sGC (11, 12), albeit their exact physiological role remains to be determined (13).

An important issue for understanding sGC activation and deactivation mechanisms is the identification of structural states and transitions, which can be addressed respectively by x-ray diffraction and by time-resolved spectroscopy. For example, after ligand release from the heme, fast protein structural relaxation can be detected in myoglobin (14). To reveal conformational changes due to subunits interaction, it is necessary to compare the structural dynamics of the full-length sGC with those of a single subunit or part of subunit, namely, a functional domain. If the structural conformation of the heme domain is not strictly the same for full-length protein *versus* isolated domain, then the diatomic ligand dynamics will be modified. It is established that the dynamics of a diatomic ligand within the protein core is highly sensitive to the heme pocket conformation and to strains on the heme iron through the proximal histidine, which imposes energy barriers to diatomic motion (15–17). Here, we compared the dynamic interaction of NO and CO within the full-length sGC and the isolated human heme domain of the β_1-subunit, restricted to the first 190 amino acids, referred to as β_1(190) hereafter. We have chosen this a sequence length because sGC is often compared with bacterial H-NOX sensors having such length, homologous to the sGC heme domain, for investigating its activation. It is thus pertinent to investigate ligand dynamics in an isolated heme domain whose length is same as the bacterial NO sensors used as sGC models. In the present study, to investigate the interaction of

* This work was supported by a Fondation pour la Recherche Médicale fellowship (to B.-K. Y.).
[S] This article contains supplemental Tables S1 and S2, Figs. S1–S5, and additional references.
[1] To whom correspondence should be addressed. Tel.: 331-69-33-50-52; Fax: 331-69-33-50-84; E-mail: michel.negrerie@polytechnique.fr.
[2] The abbreviations used are: sGC, soluble guanylate cyclase; β_1(190), heme domain from sGC β-subunit comprising the first 190 amino acids; 4c, 4-coordinate; SVD, singular value decomposition.

diatomics within the proteins, we have probed the dynamics of the ligands NO and CO after photo-dissociation from the heme by piconanosecond absorption spectroscopy. This approach is based on the photo-dissociation of NO (or CO) previously bound to the heme and then to probe the sGC/NO dynamics and interaction when NO is unbound, but still moving within the protein core. In other words, photo-dissociating a diatomic from the heme with a fast laser pulse allows to shift the equilibrium Fe−NO ↔ Fe+NO whose evolution is probed.

EXPERIMENTAL PROCEDURES

Purification of Soluble Guanylate Cyclase and Sample Preparation—sGC was purified from bovine lung by chromatography, and its activity was assayed as described previously (18). sGC was obtained directly in the ferrous state after the last column (λ_{max} = 431 nm). The final buffer was 25 mM triethanolamine, 50 mM NaCl, 1 mM DTT, 1 mM $MgCl_2$, pH 7.4. An aliquot of sGC in buffer (70 μl at ~20 μM) were put in a quartz cell (1-mm optical path length) sealed with a rubber stopper and degassed with four cycles of vacuuming and purging with argon (Air Liquide, 99.999%) so that O_2 was removed completely. For preparing NO-liganded sGC, gas phase NO diluted to 1% in N_2 (Air Liquide) was directly introduced in the vacuumed spectroscopic cell through the gas train, yielding 20 μM of NO in the aqueous phase. Full equilibration was obtained by waiting 20 min with the cell still connected to the gas train, ensuring an "infinite" reservoir of NO to avoid NO depletion. Then, a second stopper in silicone, with vacuum grease, was stacked on the cell. Steady-state absorption spectra (Shimadzu 1601 spectrophoto-meter) were recorded for monitoring the evolution of NO binding and also after the laser measurements to verify the state of the sample. The absorbance of the nitrosylated sGC samples was in the range 0.2–0.3 at the maximum of the Soret band. For the CO-liganded samples, we introduced gas phase 100% CO directly in the degassed cell.

Preparation of Isolated Heme Domain—The isolated domain β_1(190) has a sequence strictly identical for both human and bovine species. Expression of isolated heme domain of human sGC was performed at Laboratoire de Toxicologie et Pharmacologie (INSERM, UMR-S747, Paris, France) as described in Ref. 8. The isolated heme domain (in 50 mM triethanolamine, 300 mM NaCl, 5% glycerol, pH 8.2) was prepared for spectroscopy similarly as sGC, except a supplementary step of reduction: after vacuuming, a 10-μl aliquot of sodium dithionite (5 mM) was introduced into the cell with a gas-tight syringe to obtain final concentration of 0.5 mM. The reduction of heme was monitored by measuring the spectrum before adding 10% NO (200 μM in aqueous phase) in the same way as performed with sGC.

Time-resolved Absorption Spectroscopy—Time-resolved picosecond absorption was performed using the pump probe laser system described previously (19). The photo-dissociation of NO was achieved with an excitation pulse at 564 nm whose duration was ~40 fs with a repetition rate of 30 Hz. The broad spectrum probe pulse was generated by means of a continuum. The transient absorption spectrum after a variable delay between pump and probe pulses was recorded with a CCD detector coupled to a spectrometer. The same sample quartz cell (1-mm optical path length) was used for recording the equilibrium spectra and the transient absorption. The temperature was 18 °C during all measurements. Up to 50 scans were averaged.

Analysis of Transient Spectra and Kinetics—Transient spectra were recorded simultaneously with kinetics as a time-wavelength matrix data whose global analysis was performed by singular value decomposition (SVD) of the matrix (19) to retrieve individual spectral components evolving with different time constants. Each SVD kinetic component associated with a particular SVD spectrum was fit to a sum of a minimum number of exponentials: $\Sigma_i A_i(\exp(-t/\tau_i)) + C$. However, because the induced absorption from four-coordinate heme and absorption decrease from the six-coordinate NO-liganded β_1(190) species were overlapping strongly, it appeared difficult to separate the signal of both processes by means of SVD in the case of β_1(190)-NO. Therefore, we performed analysis of individual kinetics at particular wavelengths. sGC-NO data were fitted by both procedures and CO data for both proteins were analyzed by SVD. In each case, a 4-ps component was included in the fitting function to take into account the initial decay of vibrational excited states (19).

Bimolecular Rebinding: Nanosecond to Millisecond Time-resolved Absorption—We measured the bimolecular CO rebinding by flash photolysis (rather than by stopped-flow) to detect any additional rebinding phases. We have used a home-built spectrophotometer with an extended time-range for detection, from 5 ns to 1 s, based on two lasers, which are delayed electronically (20). The photo-dissociating pulse, whose duration (~5 ns) determines the time resolution, is tuned at 532 nm in the Q-band of the heme. The probing pulse, provided by a tunable optical parametric oscillator, is tuned at 450 nm to probe the kinetics of differential absorption due to the disappearance of 5-coordinate dissociated heme. The electronic time delay after the dissociating pulse was changed linearly from 1 ns to 30 ns, then was changed with a half-$\log_{10}$ progression from 30 ns to 0.1 s. Eight scans were averaged for each kinetics. The same concentrations were used for the picosecond and for the nano-to-millisecond measurements.

RESULTS AND DISCUSSION

Picosecond Dynamics of NO—In the presence of NO, nitrosylated sGC is 100% 5-coordinate-NO (5c-NO), as shown by its steady-state absorption maximum at 399 nm (Fig. 1*A*). Consequently, the transient spectra after NO photo-dissociation from sGC (Fig. 1*B*) shows an induced absorption due to the 4-coordinate (4c) heme together with a bleaching at 396 nm due to disappearance of 5c-NO heme (17, 18). The NO geminate rebinding kinetics to the 4c heme (Fig. 1*C*) is very fast (7.5 ± 0.3 ps) with high yield (96 ± 1%), as already observed (17, 18). The isolated β_1(190) is also 5-coordinate in the presence of NO (Fig. 1*D*). This ligation is not 100%, similarly with the homologous domain β_1(1–189) from the cyanobacteria *Nostoc* sp. (11), but contrary to the slightly longer domain from rat β_1(1–194) (21) and to the full-length sGC. A shoulder at 425 nm indicates that ~10–15% of β_1(190) main be unliganded or bis-ligated with an internal side chain. The ligation with CO yields 100% of 6-co-

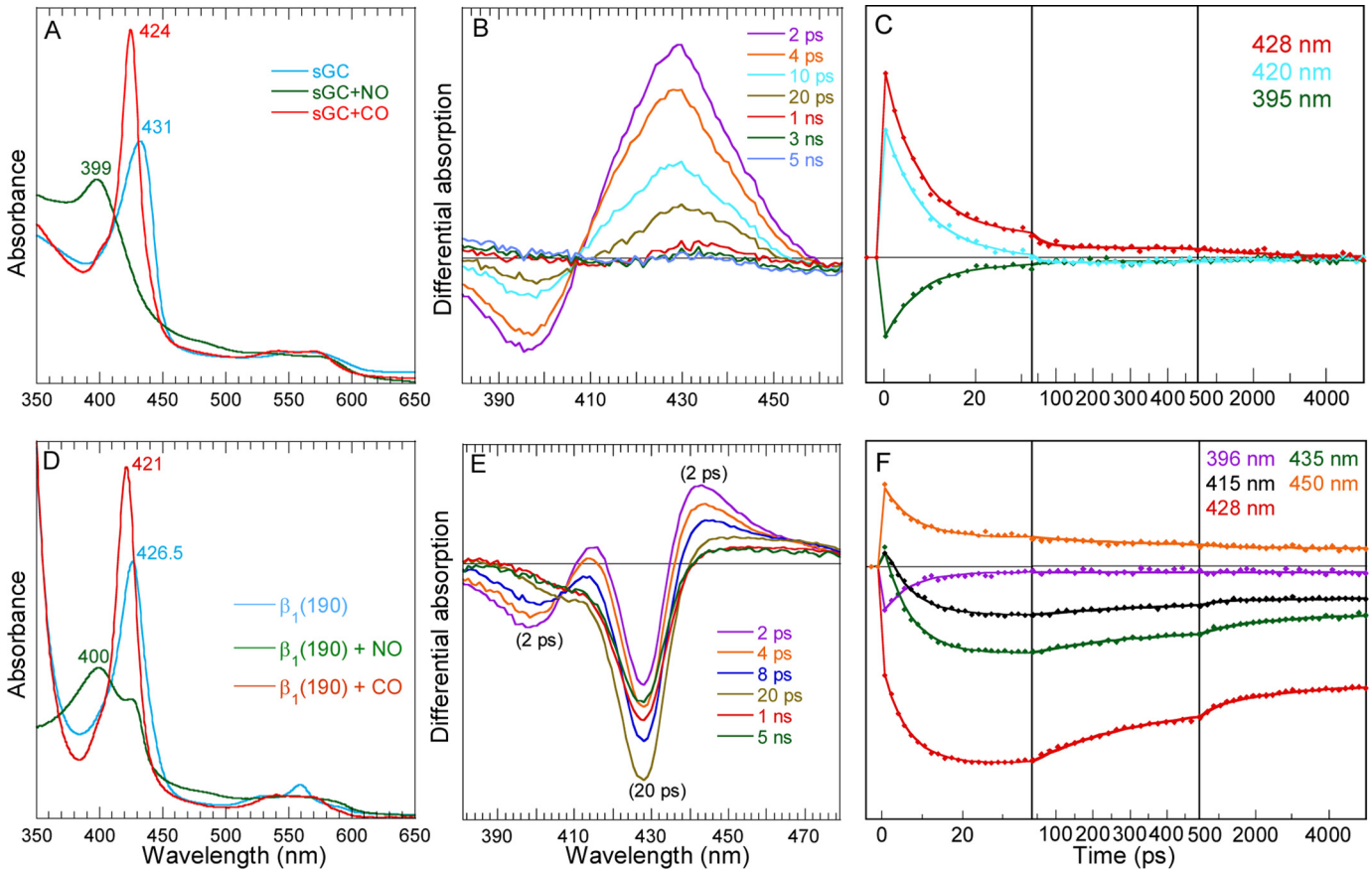

FIGURE 1. **Dynamics of NO after photo-dissociation from the entire sGC and from the isolated heme domain β_1(190).** *A*, steady-state spectra of unliganded sGC and liganded with NO and CO. *B*, transient spectra at selected time delays after photo-dissociation of NO from full-length sGC. *C*, kinetics of NO rebinding to sGC at selected wavelengths. *D*, steady-state spectra of unliganded isolated heme domain β_1(190) and liganded with NO and CO. The slope below 360 nm is due to the absorption of dithionite (0.5 mM) used as reductant. *E*, transient spectra at selected time delays after photo-dissociation of NO from β_1(190). *F*, kinetics of NO rebinding to β_1(190) at selected wavelengths fitted to a sum of exponentials. The averaged fitted parameters are given in Table 1 (Global SVD analysis in supplemental Fig. S1 and individual parameters in supplemental Table S1).

ordinate form, as observed for rat β_1(1–194) (21) and *Nostoc* sp. β_1(1–189) (11).

The comparison of the raw transient spectra for β_1(190) (Fig. 1*E*) and for sGC immediately reveals different processes in both proteins. In the case of isolated β_1(190), the presence of two bleaching minima at +2 ps indicates that two species were initially photo-induced. The first bleaching (398 nm), also present in sGC spectra, is assigned readily to the disappearance of 5c-NO species yielding the 4c heme, whose decrease is due to NO rebinding. The second bleaching (428 nm), not located at the Soret position observed for 6c-NO heme of nitrosylated myoglobin (420 nm) or homologous NO sensor (22), is due to the disappearance of the reduced unliganded heme (5c-His). Its position is same as the shoulder in the steady-state spectrum of NO-liganded species (Fig. 1*D*). We now discuss its assignment.

Because the reduced 5c-His species disappears immediately (<1 ps) upon photo-excitation in presence of NO, we verified whether the same effect occurs also in absence of NO, in anaerobic conditions (Fig. 2 and supplemental Table S2). In this case, the behavior of transient spectra is very different from that of a pure relaxation of excited states, which is very fast and has an isosbestic point shifting in the opposite direction (18). In absence of NO, the difference of transient spectra shape at +2 ps and +5 ns indicates that two processes occurred after photo-excitation: fast relaxation of excited states of the vibrationally hot heme is identified by the fast spectral shift (19) with τ_{ex} = 4.3 ps (Fig. 2*A*). Second, the same component is identified by the bleaching centered at 428 nm, exactly as observed in the case of nitrosylated β_1(190) (Fig. 1*E*). Remarkably, the major spectral component from global analysis is identical in absence and presence of NO (supplemental Fig. S1*C* and Fig. 2*C*), demonstrating that its origin cannot be NO geminate rebinding. Because 5c-His cannot be photo-dissociated with a 564-nm laser pulse, we therefore assigned this effect to photo-oxidation, which can occur both in presence and absence of heme-bound NO. The comparison of steady-state spectra of the sample immediately before and after laser experiment (supplemental Fig. S2) shows that they are identical and no accumulation of ferric heme is observed, so that re-reduction took place after photo-oxidation.

The similarity of transient spectra at +5 ns in the presence and absence of NO and the absence of another spectral component indicate that the reduction process is identical in both cases, and only the time constants are influenced by the presence of NO. In β_1(190)-NO, reduction occurs simultaneously with NO rebinding to 4c heme due to dissociated 5c-NO, producing complex kinetics (Fig. 1*F*). The broad bleaching due to oxidation of 5c-His heme, centered at 428 nm (Fig. 1*E*), largely

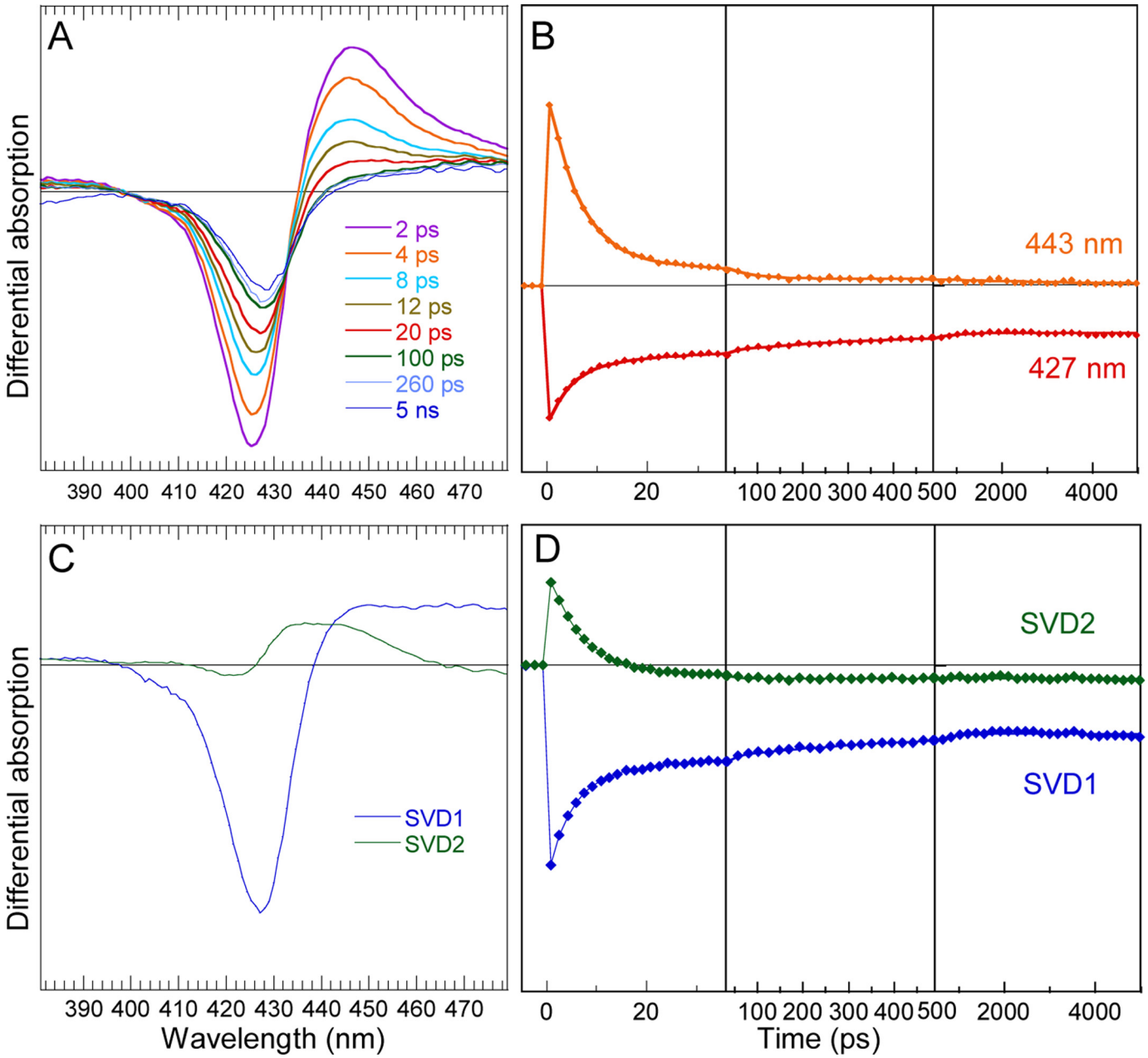

FIGURE 2. **Excited states dynamics in reduced unliganded β_1(190) heme domain.** *A*, transient spectra at various time delays. *B*, kinetics at maximum of induced absorption and at minimum of bleaching. *C*, spectral components from global SVD analysis of the entire time-wavelength matrix. *D*, kinetic components from SVD analysis (fitted parameters are given in supplemental Table S2).

overlaps the induced absorption of 4c heme as seen in sGC (Fig. 1*B*). Consequently, NO rebinding to the 4c heme provokes an initial decrease of absorption at 428 nm until 20 ps (Fig. 1*F*), followed by an increase due to back-reduction of the 5c-His heme. Kinetics were fitted at particular wavelengths (Table 1), and individual spectral contributions from different processes were obtained by global analysis (supplemental Fig. S1*C*).

Fitting the β_1(190)-NO kinetics resulted in three exponential components: the 7-ps component is due to NO rebinding to the 4c heme, which does not have an energy barrier, similarly to entire sGC, whereas the slower components (τ_2 = 230 ps and τ_3 = 2 ns) are assigned to the heme reduction after photo-oxidation because they are associated with a decrease of the bleaching at 428 nm. The respective contribution to the absorption kinetics from NO rebinding after photo-dissociation and from reduction after photo-oxidation are compared in supplemental Fig. S3. The back-reduction in presence of NO proceeds with several phases (time constants from fitted kinetics in supplemental Table S2) as it does in the absence of NO, but with modified time constants. The electron donor for this fast reduc-

TABLE 1
Time constants τ_i and relative amplitudes A_i of exponential component from fitted kinetics in Figs. 1 and 4

Species	τ_1 (A_1)	τ_2 (A_2)	τ_3 (A_3)	A_4 (constant)
sGC-NO	7.5 ps (0.96)			0.04
β_1-NO	7.0 ps (0.33)	230 ps (0.17)	2.0 ns (0.12)	0.38
sGC-CO			≥1 ns (0.02)	0.98
β_1-CO	35 ps (0.13)	171 ps (0.20)	≥1 ns (0.18)	0.49

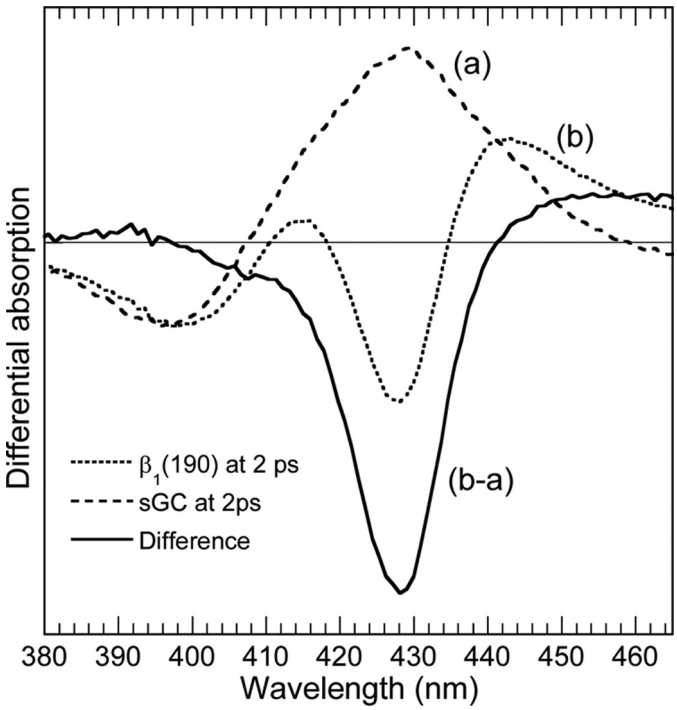

FIGURE 3. **Calculated difference transient spectra of the photo-oxidized β_1(190) heme at +2 ps (*solid line*) obtained by subtracting the raw transient spectra of sGC (*dashed line*), containing only the contribution of NO photo-dissociation, from the raw spectra of photo-excited β_1(190)-NO (*dotted line*) containing both the contributions of NO photo-dissociation and photo-oxidation.** The raw spectra were normalized at the minimum of the bleaching (396 nm). This calculated spectrum is remarkably similar to that of unliganded of β_1(190) (Fig. 2*C*) and to that of SVD1 components for β_1-NO (supplemental Fig. S1*C*).

tion is probably the electron acceptor of initial photo-oxidation, which we did not attempt to identify here because we did not aim at investigating the heme photo-oxidation process but the consequences of heme domain isolation. However, the large constant term (38%) associated with photo-oxidation suggests that back-reduction (back electron transfer from acceptor/donor) has an energy barrier.

Both processes, NO geminate rebinding and back-reduction after photo-oxidation, are initiated immediately and simultaneously from electronic excited state. We demonstrate this by showing that in β_1(190), the signature of photo-oxidation is already present at +2 ps, that is to say, after the decay of electronic excited state (< 1 ps). We calculated the difference spectrum of photo-oxidation immediately after photo-excitation (+2 ps) by subtracting the raw transient spectra of sGC at +2 ps (which contains only the contribution of NO dissociation) from the raw spectra of β_1(190) at +2 ps, which contains the contributions of both photo-oxidation and NO photo-dissociation. The resulting difference transient spectrum (Fig. 3), free from the contribution of NO dissociation, is that of the photo-oxidized heme at +2 ps. Remarkably, it is identical to the spectra at +5 ns, both in absence (Fig. 2*A*) and in presence (Fig. 1*E*) of NO, and identical to the major spectral components obtained from global analysis of the data (Fig. 2*C* and supplemental Fig. S1*C*). This clearly shows that the bleaching due to photo-oxidation hides the induced absorption of 4c heme due to NO photo-dissociation. This also demonstrates that the second process occurring immediately upon photo-excitation of β_1(190)-NO does not involve NO dynamics. It must be noted that the photo-oxidation transient spectrum is similar to the difference spectra of autooxidation of the β_1(1–217) fragment (21) in the presence of O_2, whereas in β_1(1–194) the larger absorption shifted toward 410 nm (21) suggests that ferric heme became liganded with OH^- from solution, a process that is not faster than ~0.1 μs (23). All kinetics are depicted together in the last figure.

Other heme proteins than sGC can form a 5c-NO species with the cleavage of the Fe-His bond, in particular the bacterial cytochrome *c*′. Since the discovery that NO binds to the proximal side of the heme in cytochrome *c*′ (24), several models have included sGC with proximal 5c-NO. However, the diffusion of NO from one side of the heme to the other (or from solution) is expected to occur in a time range longer than 5 ns, so that under geminate rebinding condition, a second NO reaction, as well as the formation or not of a proximal 5c-NO heme, cannot be at the origin of the differences observed between β_1(190)-NO and sGC-NO.

From our observations, we conclude that the complementary part (191–619) of the β-subunit and/or the α-subunit exert strains which modulate the heme redox properties. Excluding these protein domains changes the strains on the heme and may modify the heme distortion, which has been shown to change the redox potential (25, 26). This likely explains the photo-oxidation (charge transfer) induced by heme electronic excited states promotion and the 4-nm shift of the 5c-His Soret maximum with respect to full-length sGC through a subtle change of electronic orbital overlap.

In this line, it was pointed out by Karow *et al.* (21) that rat β_1(1–194) is not as stable as sGC. Remarkably, they observed (21) that "the rate of oxidation to Fe^{3+} is very slow for sGC and occurs much more quickly in β_1(1–194)." Also, the kinetics of NO dissociation from rat heme domain β_1(1–194) (27) and kinetics of NO binding to bacterial *Nostoc* NO sensor (sequence 1–183) (13) are different from those of entire sGC. This conformational difference may also explain the observation that the same single mutation (I145Y) does not induce O_2 binding affinity in the full-length sGC (10, 28) as it does in the β_1(1–385) construct (29), whereas a homologous bacterial NO sensor possesses a high O_2 affinity (30).

Picosecond Dynamics of CO—We now see that photo-oxidation does not occur when the heme is 6-coordinate in the presence of CO, which activates sGC only 2.5- to 4-fold (31, 32). The steady-state spectra of sGC and β_1(190) liganded with CO are similar but the Soret maximum is shifted by 3 nm (supplemental Fig. S4*A*), indicating different constraints exerted on the heme. We measured the dynamics of CO in isolated β_1(190) compared with the full-length sGC. The transient difference spectra (Fig. 4, *A* and *B*) do not show a shift of isosbestic points for both proteins, meaning that only one process takes place, *i.e.* the geminate rebinding of photo-dissociated CO to the 5c-His, which is readily identified by the position of the bleaching at 6c-CO Soret wavelength (supplemental Fig. S4*B*). The conspicuous decrease of the amplitude of transient spectra of β_1(190) after CO dissociation indicates fast CO rebinding in the picosecond and nanosecond time ranges. Whereas the shape of their transient spectra is the same, the kinetics of CO rebinding

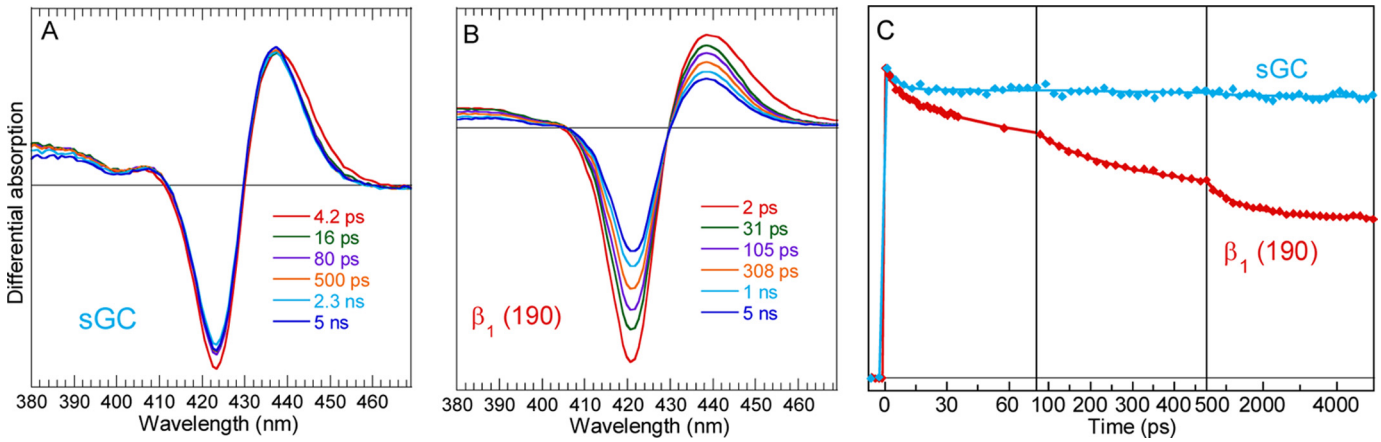

FIGURE 4. **Dynamics of CO after photo-dissociation from the entire sGC and from the isolated heme domain β_1(190).** *A*, transient spectra at selected time delays after photo-dissociation of CO from full-length sGC. *B*, transient spectra at selected time delays after photo-dissociation of CO from β_1(190). *C*, kinetics of CO geminate rebinding to sGC compared with β_1(190) calculated by global analysis, representing the evolution of the entire difference spectrum. A 4-ps component was included in the fitting function to take into account the initial excited states decay.

are dramatically different for sGC and β_1(190). For sGC, only a very small amplitude of CO rebinding (2%) occurs with a time constant ≥1 ns, but no further CO rebinding is observed (Fig. 4*C*). Contrastingly, in the heme domain β_1(190) 51% of CO rebind up to 5 ns with three phases (time constants in Table 1) quite similarly with the kinetics observed for NO in endothelial NO synthase with multiple energy barriers (15). Also, the oxidation propensity, observed with NO, is remarkably not observed in the presence of CO. Thus, it cannot originate from increased solvent exposure.

As deduced by the fast CO geminate components (35 and 171 ps) the conformation adopted by β_1(190) induces less constraints on the proximal His than in full-length sGC. The photo-dissociated 5-coordinate heme adopts a more planar conformation, which leads to a decrease of energy barrier for CO rebinding (33). As a consequence, the Fe-CO bond formation in β_1(190) competes with CO diffusion out of the heme pocket. In line with this result, Raman data on mutated Hb (34) and heme-substituted Hb (35) support the idea that internal strains induced by the quaternary structure modulate the strain on the iron.

The strain on the proximal His (or/and the distortion of the heme) decreased as a consequence of the absence of α-subunit and β_1(191–619) domains interacting with β_1(190). The decrease of this strain induces a position of the iron closer to the heme plane and consequently decreases the energy barrier for CO rebinding (16, 34).

Bimolecular Rebinding of CO —Conformational changes can influence the energy barrier for CO diffusion between the heme pocket and the solvent, as observed for Mb (36) and Hb (37) mutants. We thus measured on an extended time scale the kinetics of CO bimolecular rebinding to sGC and to β_1(190) after CO photo-dissociation with a 5-ns pulse, in the presence of [CO] = 1.33 mM (Fig. 5). For both proteins, an immediate decay is observed within the time resolution (unresolved picosecond components) and an additional slow geminate rebinding is observed with time constant τ_4 = 18 ns for β_1(190), more important than for sGC. Then, a slow geminate phase occurs before CO bimolecular rebinding, assigned to CO still in the protein core, but outside the heme pocket, whose time constant

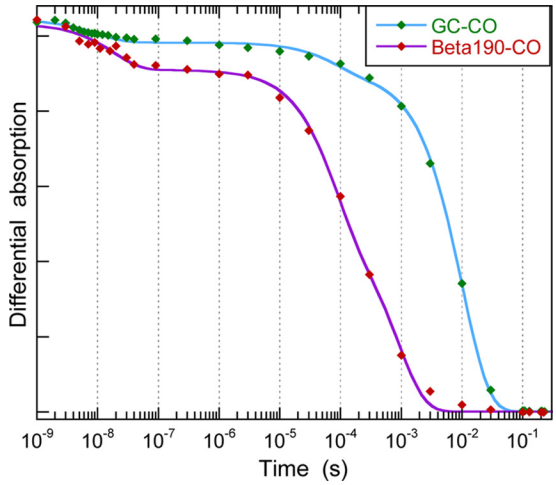

FIGURE 5. **Bimolecular rebinding of CO to full-length sGC and to β_1(190) after CO photo-dissociation.** The differential absorption kinetics were probed at 450 nm and are normalized. The fast minor decay at ~10–20 ns is due to CO geminate rebinding, including the picosecond phase. The slower phase, with much larger amplitude, is the bimolecular rebinding of CO. The data were fitted to a sum of three exponentials, and the fitted time constants are listed in Table 2. The maximum of the signal corresponds to the temporal coincidence of the photo-dissociating and probing pulses. The pressure of pure CO in the gaseous phase above the sample is 1.3 bar, yielding a concentration of 1.33 mM in the aqueous phase at 20 °C.

τ_{gem2} = 80 μs is same for sGC and β_1(190) but with very different relative amplitudes (Table 2). Bimolecular rebinding is observed in the millisecond range and is remarkably faster for β_1(190) (τ_{bi} = 0.9 ms) than for sGC (τ_{bi} = 10 ms). The concentration of CO in the sample buffer was 1.33 mM, yielding bimolecular association constants $k_{on} = 0.075 \times 10^6$ $M^{-1}\cdot s^{-1}$ for sGC and 0.83×10^6 $M^{-1}\cdot s^{-1}$ for β_1(190). The value for sGC-CO association is twice that measured by stopped-flow (0.036×10^6 $M^{-1}\cdot s^{-1}$; 38). Remarkably, the k_{on} rate for β_1(190) is of same order of magnitude as that of myoglobin measured by the same method (supplemental Fig. S5 and Table 2) but is 11-fold faster than that of sGC. We assigned the differences in CO picosecond-nanosecond dynamics between sGC and β_1(190) to relaxed conformational constraints in the isolated heme domain. The larger k_{on} for β_1(190) may be additionally attributed to removal of steric barriers due to the absence of α-sub-

TABLE 2
Time constants τ_i and relative amplitudes A_i of exponential component in fitted kinetics in Fig. 5

Species	τ_{gem1} (A_1)	τ_{gem2} (A_2)	τ_{bi} (A_{bi})	k_{on}[a]
				$_{M^{-1}\cdot s^{-1}}$
sGC-CO	10 ± 2 ns (0.05)	80 ± 2 μs (0.08)	10 ± 0.2 ms (0.87)	0.075 ± 0.01 × 10^6
β_1(190)-CO	18 ± 4 ns (0.12)	80 ± 10 μs (0.40)	0.9 ± 0.1 ms (0.48)	0.83 ± 0.1 × 10^6
Mb-CO		0.5 ± 0.2 μs (0.02)	0.6 ± 0.02 ms (0.98)	1.25 ± 0.1 × 10^6

[a] Association rate constants calculated with [CO] = 1.33 mM.

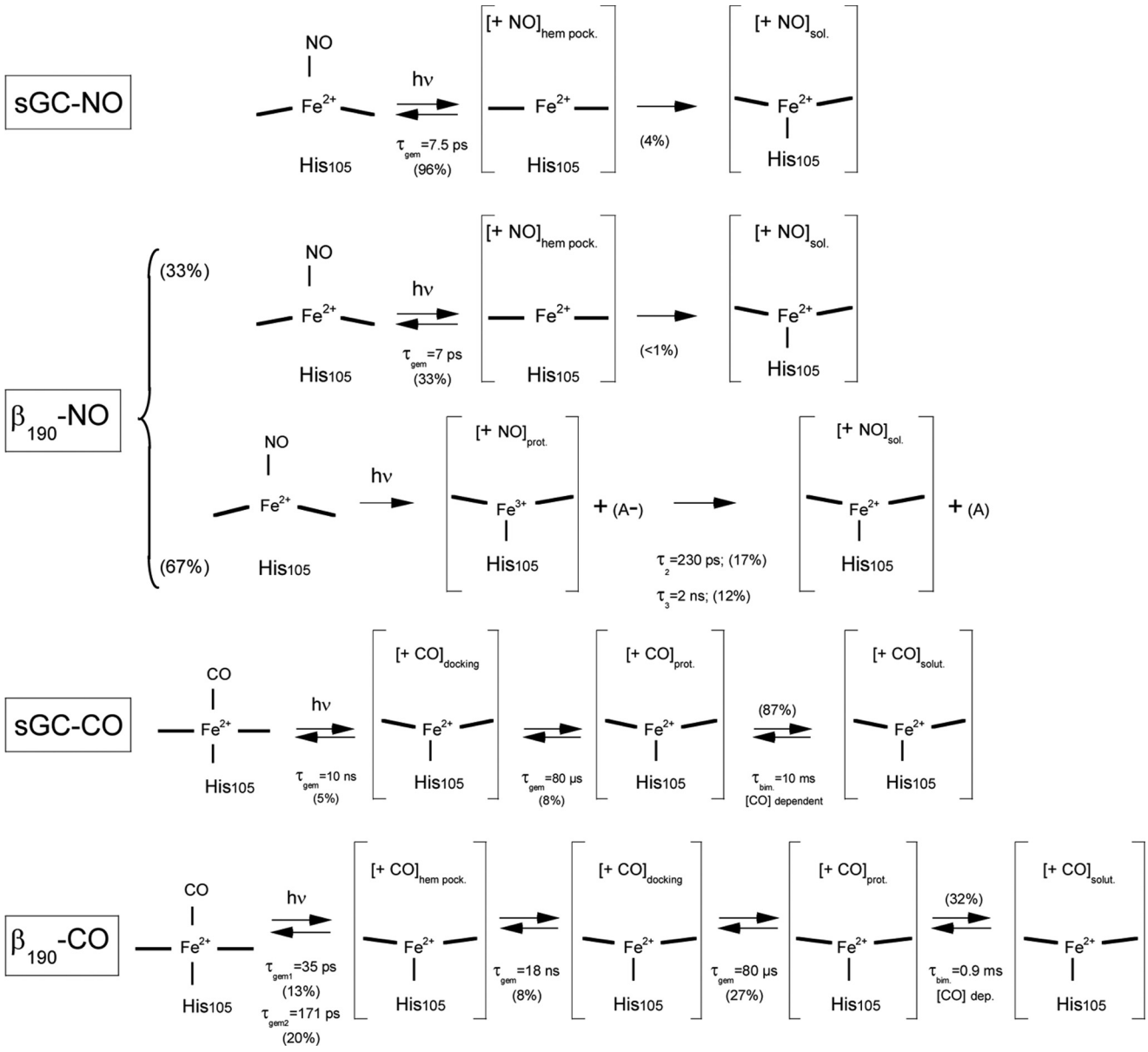

FIGURE 6. **Summary of transitions observed after photo-excitation of sGC and β_1(190) liganded with NO and CO.** For β_1(190)-CO, the amplitudes were calculated relatively to the picosecond components, assuming that only components A_3 and A_4 from picosecond kinetics can be detected in the extended time range kinetics. "A" is unidentified electron acceptor. The *subscripts* indicate NO and CO located in heme pocket (*hem. pock.*), docking site (*docking.*), protein core (*prot.*), or solution (*sol.* or *solut.*).

unit and other domains of the β-subunit. The various observed transitions are summarized in Fig. 6.

The similarity of $\tau_{gem2} = 80$ μs for both proteins is noteworthy as its amplitude is increased. We assigned it to a phase of geminate rebinding of CO located in an intermediate protein site between heme pocket and solution, albeit some myoglobin mutants have a time constant close to this value for bimolecular CO rebinding (36, 39) because in these cases, Mb-CO kinetics did not show any other component attributable to bimolecular association, contrary to sGC. The fast k_{on} rate for β_1(190) explains that this site is more populated than in sGC and induces a larger amplitude of this geminate phase. It thus appears that the CO rebinding ps-ns phases are modulated by proximal strains and the μs phase and k_{on} barriers can also be influenced in a steric manner by the absence of the other protein domains.

The modification of CO dynamics together with the increased oxidation propensity in the isolated heme domain with respect to the full-length sGC demonstrates that the distortion and strains on the heme are not identical in both cases. This is in line with the lower stretching ν_{CO} frequency in β_1(1–194) than in sGC (21). This implies that constraints exist between both subunits and between the heme domain and the remaining part of β-subunit β_1(191–619), ensuring that the energy relaxation due to Fe^{2+}-His bond breaking is transmitted to the catalytic site in dimeric sGC. Thus, in the absence of the catalytic α-subunit and other β-subunit domains, these constraints are relaxed, so that the isolated heme domain could be in a conformational state much closer to the activated state, even in absence of NO, than when incorporated in the entire protein. Following the example of hemoglobin (40), the unliganded dimeric sGC appears in a "tensed" state maintained by the Fe^{2+}-His bond, and NO-liganded sGC appears in a "relaxed" state.

In summary, in reduced unliganded β_1(190), photo-oxidation occurs with back-reduction from an internal acceptor, contrary to sGC, but fast NO rebinding occurs like in sGC. In β_1(190)-CO, the CO rebinding is much faster than in sGC, but without photo-oxidation. The isolated heme domain β_1(190) has a different reactivity than inserted in the full-length dimeric sGC due to a considerably decreased proximal strain on the heme in the absence of other domains and α-subunit. Thus, functional models derived from isolated heme domain (41) and, *a fortiori*, structural models from homologous bacterial NO sensors (11) may not apply directly to modeling the activation mechanism in native dimeric sGC. These observations reflect the plasticity of the H-NOX heme domain, which is influenced, apart from variations of its own sequence, by the presence of interacting domains and subunits involved in allostery, so that not only the dynamics of diatomic ligands can be controlled but also the heme redox properties (13, 25, 26).

Acknowledgments—We thank Pierre Nioche (INSERM, UMR S747) for providing us with the overexpressed sGC heme domain and Fabrice Rappaport (CNRS, UMR 7141) for enabling us to measure the extended time range dynamics with spectroscopic setup.

REFERENCES

1. Murad, F. (1999) Discovery of some of the biological effects of nitric oxide and its role in cell signaling (Nobel lecture). *Angew. Chem. Int. Ed.* **38,** 1857–1868
2. Ignarro, L. J., Buga, G. M., Wood, K. S., Byrns, R. E., and Chaudhuri, G. (1987) Endothelium-derived relaxing factor produced and released from artery and vein is nitric oxide. *Proc. Natl. Acad. Sci. U.S.A.* **84,** 9265–9269
3. Palmer, R. M., Ferrige, A. G., and Moncada, S. (1987) Nitric oxide release accounts for the biological activity of endothelium-derived relaxing factor. *Nature* **327,** 524–526
4. Bian, K., Doursout, M. F., and Murad, F. (2008) Vascular system: role of nitric oxide in cardiovascular diseases. *J. Clin. Hypertens.* **10,** 304–310
5. Coggins, M. P., and Bloch, K. D. (2007) Nitric oxide in the pulmonary vasculature. *Arterioscler. Thromb. Vasc. Biol.* **27,** 1877–1885
6. Nagy, G., Clark, J. M., Buzás, E. I., Gorman, C. L., and Cope, A. P. (2007) Nitric oxide, chronic inflammation and autoimmunity. *Immunol. Lett.* **111,** 1–5
7. Deinum, G., Stone, J. R., Babcock, G. T., and Marletta, M. A. (1996) Binding of nitric oxide and carbon monoxide to soluble guanylate cyclase as observed with Resonance raman spectroscopy. *Biochemistry* **35,** 1540–1547
8. Nioche, P., Berka, V., Vipond, J., Minton, N., Tsai, A. L., and Raman, C. S. (2004) Femtomolar sensitivity of a NO sensor from *Clostridium botulinum*. *Science* **306,** 1550–1553
9. Pellicena, P., Karow, D. S., Boon, E. M., Marletta, M. A., and Kuriyan, J. (2004) Crystal structure of an oxygen-binding heme domain related to soluble guanylate cyclases. *Proc. Natl. Acad. Sci. U.S.A.* **101,** 12854–12859
10. Boon, E. M., Huang, S. H., and Marletta, M. A. (2005) A molecular basis for NO selectivity in soluble guanylate cyclase. *Nat. Chem. Biol.* **1,** 53–59
11. Ma, X., Sayed, N., Beuve, A., and van den Akker, F. (2007) NO and CO differentially activate soluble guanylyl cyclase via a heme pivot-bend mechanism. *EMBO J.* **26,** 578–588
12. Martin, F., Baskaran, P., Ma, X., Dunten, P. W., Schaefer, M., Stasch, J. P., Beuve, A., and van den Akker, F. (2010) Structure of cinaciguat (BAY 58-2667) bound to Nostoc H-NOX domain reveals insights into heme-mimetic activation of the soluble guanylyl cyclase. *J. Biol. Chem.* **285,** 22651–22657
13. Tsai, A. L., Berka, V., Martin, F., Ma, X., van den Akker, F., Fabian, M., and Olson, J. S. (2010) Is Nostoc H-NOX a NO sensor or redox switch? *Biochemistry* **49,** 6587–6599
14. Sato, A., Gao, Y., Kitagawa, T., and Mizutani, Y. (2007) Primary protein response after ligand photo-dissociation in carbonmonoxy myoglobin. *Proc. Natl. Acad. Sci. U.S.A.* **104,** 9627–9632
15. Négrerie, M., Berka, V., Vos, M. H., Liebl, U., Lambry, J. C., Tsai, A. L., and Martin, J. L. (1999) Geminate recombination of nitric oxide to endothelial nitric-oxide synthase and mechanistic implications. *J. Biol. Chem.* **274,** 24694–24702
16. Ionascu, D., Gruia, F., Ye, X., Yu, A., Rosca, F., Beck, C., Demidov, A., Olson, J. S., and Champion, P. M. (2005) Temperature-dependent studies of NO recombination to heme and heme proteins. *J. Am. Chem. Soc.* **127,** 16921–16934
17. Kruglik, S. G., Lambry, J. C., Cianetti, S., Martin, J. L., Eady, R. R., Andrew, C. R., and Negrerie, M. (2007) Molecular basis for nitric oxide dynamics and affinity with *Alcaligenes xylosoxidans* cytochrome *c*. *J. Biol. Chem.* **282,** 5053–5062
18. Négrerie, M., Bouzhir, L., Martin, J. L., and Liebl, U. (2001) Control of nitric oxide dynamics by guanylate cyclase in its activated state. *J. Biol. Chem.* **276,** 46815–46821
19. Negrerie, M., Cianetti, S., Vos, M. H., Martin, J. L., and Kruglik, S. G. (2006) Ultrafast heme dynamics in ferrous versus ferric cytochrome *c* studied by time-resolved resonance Raman and transient absorption spectroscopy. *J. Phys. Chem. B* **110,** 12766–12781
20. Beal, D., Rappaport, F., and Joliot, P. (1999) A new high-sensitivity 10-ns time-resolution spectrophotometric technique adapted to *in vivo* analysis of the photosynthetic apparatus. *Rev. Sci. Instrum.* **70,** 202–207
21. Karow, D. S., Pan, D., Davis, J. H., Behrends, S., Mathies, R. A., and Marletta, M. A. (2005) Characterization of functional heme domains from soluble guanylate cyclase. *Biochemistry* **44,** 16266–16274
22. Karow, D. S., Pan, D., Tran, R., Pellicena, P., Presley, A., Mathies, R. A., and Marletta, M. A. (2004) Spectroscopic characterization of the soluble guanylate cyclase-like heme domains from *Vibrio cholerae* and *Thermoanaerobacter tengcongensis*. *Biochemistry* **43,** 10203–10211
23. Cao, W., Christian, J. F., Champion, P. M., Rosca, F., and Sage J. T. (2001) Water penetration and binding to ferric myoglobin. *Biochemistry* **40,** 5728–5737
24. Lawson, D. M., Stevenson, C. E., Andrew, C. R., and Eady, R. R. (2000) Unprecedented proximal binding of nitric oxide to heme: implications for guanylate cyclase. *EMBO J.* **19,** 5661–5671
25. Olea, C., Jr., Kuriyan, J., and Marletta, M. A. (2010) Modulating heme redox potential through protein-induced porphyrin distortion. *J. Am. Chem. Soc.* **132,** 12794–12795
26. Olea, C., Boon, E. M., Pellicena, P., Kuriyan, J., and Marletta, M. A. (2008) Probing the function of heme distortion in the H-NOX family. *ACS Chem. Biol.* **3,** 703–710
27. Winger, J. A., Derbyshire, E. R., and Marletta, M. A. (2007) Dissociation of nitric oxide from soluble guanylate cyclase and heme-nitric oxide/oxygen binding domain constructs. *J. Biol. Chem.* **282,** 897–907

28. Martin, E., Berka, V., Bogatenkova, E., Murad, F., and Tsai, A. L. (2006) Ligand selectivity of soluble guanylyl cyclase: Effect of the hydrogen-bonding tyrosine in the distal heme pocket on binding of oxygen, nitric oxide, and carbon monoxide. *J. Biol. Chem.* **281,** 27836–27845
29. Derbyshire, E. R., Deng, S., and Marletta, M. A. (2010) Incorporation of tyrosine and glutamine residues into the soluble guanylate cyclase heme distal pocket alters NO and O_2 binding. *J. Biol. Chem.* **285,** 17471–17478
30. Weinert, E. E., Plate, L., Whited, C. A., Olea, C., Jr., and Marletta, M. A. (2010) Determinants of ligand affinity and heme reactivity in H-NOX domains. *Angew. Chem. Int. Ed. Engl.* **49,** 720–723
31. Stone, J. R., and Marletta, M. A. (1994) Soluble guanylate cyclase from bovine lung: activation with nitric oxide and carbon monoxide and spectral characterization of the ferrous and ferric states. *Biochemistry* **33,** 5636–5640
32. Brüne, B., Schmidt, K. U., and Ullrich, V. (1990) Activation of soluble guanylate cyclase by carbon monoxide and inhibition by superoxide anion. *Eur. J. Biochem.* **192,** 683–688
33. Ye, X., Yu, A., Georgiev, G. Y., Gruia, F., Ionascu, D., Cao, W., Sage, J. T., and Champion, P. M. (2005) CO rebinding to protoheme: Investigations of the proximal and distal contributions to the geminate rebinding barrier. *J. Am. Chem. Soc.* **127,** 5854–5861
34. Peterson, E. S., and Friedman, J. M. (1998) A possible allosteric communication pathway identified through a resonance Raman study of four β37 mutants of human hemoglobin A. *Biochemistry* **37,** 4346–4357
35. Balakrishnan, G., Ibrahim, M., Mak, P. J., Hata, J., Kincaid, J. R., and Spiro, T. G. (2009) Linking conformation change to hemoglobin activation via chain-selective time-resolved resonance Raman spectroscopy of protoheme/mesoheme hybrids. *J. Biol. Inorg. Chem.* **14,** 741–750
36. Sugimoto, T., Unno, M., Shiro, Y., Dou, Y., and Ikeda-Saito, M. (1998) Myoglobin mutants giving the largest geminate yield in CO rebinding in the nanosecond time domain. *Biophys. J.* **75,** 2188–2194
37. Birukou I., Soman, J., and Olson, J. S. (2011) Blocking the gate to ligand entry in human hemoglobin. *J. Biol. Chem.* **286,** 10515–10529
38. Stone, J. R., and Marletta, M. A. (1995) The ferrous heme of soluble guanylate cyclase: Formation of hexacoordinate complexes with carbon monoxide and nitrosomethane. *Biochemistry* **34,** 16397–16403
39. Huang, X., and Boxer, S. G. (1994) Discovery of new ligand binding pathways in myoglobin by random mutagenesis. *Nat. Struct. Biol.* **1,** 226–229
40. Perutz, M. F. (1970) Stereochemistry of cooperative effects in hemoglobin. *Nature* **228,** 726–739
41. Zhong, F., Wang, H., Ying, T., Huang, Z. X., and Tan, X. (2010) Efficient expression of human soluble guanylate cyclase in *Escherichia coli* and its signaling-related interaction with nitric oxide. *Amino Acids* **39,** 399–408